Report

Cell Reports

Physiological Plasticity of Neural-Crest-Derived Stem Cells in the Adult Mammalian Carotid Body

Graphical Abstract

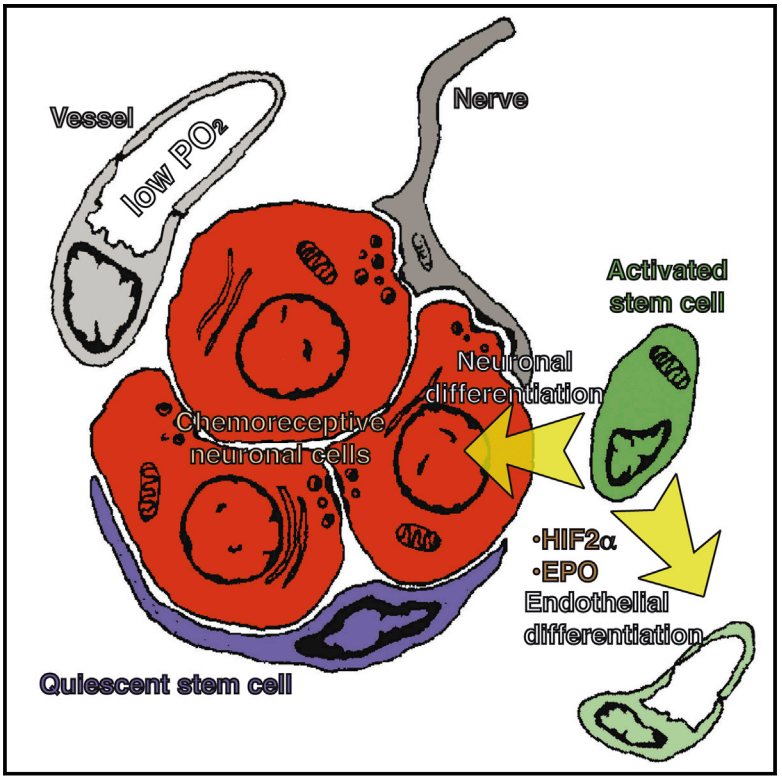

Highlights

- Adult carotid body stem cells display multipotency during organ adaptation to hypoxia
- Neural-crest-derived stem cells contribute to angiogenesis in the adult carotid body
- Endothelial differentiation from carotid body stem cells is HIF2α and EPO dependent

Authors

Valentina Annese,
Elena Navarro-Guerrero,
Ismael Rodríguez-Prieto, Ricardo Pardal

Correspondence

vannese@us.es (V.A.),
rpardal@us.es (R.P.)

In Brief

Annese et al. find that neural-crest-derived stem cells residing in the adult carotid body are multipotent. These cells have the capacity to contribute to both neurogenesis and angiogenesis during organ acclimatization to hypoxia. Endothelial fate specification is achieved by intrinsic (HIF2α) and extrinsic (EPO) mechanisms.

Annese et al., 2017, Cell Reports *19*, 471–478
April 18, 2017
http://dx.doi.org/10.1016/j.celrep.2017.03.065

Cell Reports
Report

Physiological Plasticity of Neural-Crest-Derived Stem Cells in the Adult Mammalian Carotid Body

Valentina Annese,[1,*] Elena Navarro-Guerrero,[1] Ismael Rodríguez-Prieto,[1] and Ricardo Pardal[1,2,*]
[1]Departamento de Fisiología Médica y Biofísica, Instituto de Biomedicina de Sevilla (IBiS), Hospital Universitario Virgen del Rocío/CSIC/Universidad de Sevilla, Seville 41013, Spain
[2]Lead Contact
*Correspondence: vannese@us.es (V.A.), rpardal@us.es (R.P.)
http://dx.doi.org/10.1016/j.celrep.2017.03.065

SUMMARY

Adult stem cell plasticity, or the ability of somatic stem cells to cross boundaries and differentiate into unrelated cell types, has been a matter of debate in the last decade. Neural-crest-derived stem cells (NCSCs) display a remarkable plasticity during development. Whether adult populations of NCSCs retain this plasticity is largely unknown. Herein, we describe that neural-crest-derived adult carotid body stem cells (CBSCs) are able to undergo endothelial differentiation in addition to their reported role in neurogenesis, contributing to both neurogenic and angiogenic processes taking place in the organ during acclimatization to hypoxia. Moreover, CBSC conversion into vascular cell types is hypoxia inducible factor (HIF) dependent and sensitive to hypoxia-released vascular cytokines such as erythropoietin. Our data highlight a remarkable physiological plasticity in an adult population of tissue-specific stem cells and could have impact on the use of these cells for cell therapy.

INTRODUCTION

The carotid body (CB), a neural-crest-derived paired organ located in the carotid bifurcation, is the main arterial chemoreceptor in mammals and facilitates reflex hyperventilation during hypoxia (López-Barneo et al., 2001). In addition, the CB is able to undergo neurogenesis to contribute to acclimatization of the organism during a persistent hypoxia (Edwards et al., 1971; Arias-Stella and Valcarcel, 1976; Heath et al., 1982; Wang and Bisgard, 2002). We have previously shown that glia-like sustentacular, or type II, cells surrounding chemosensory neuron-like glomus cells are neural crest stem cells (NCSCs) and contribute to CB growth in hypoxia by differentiating into new glomus cells (Pardal et al., 2007; Platero-Luengo et al., 2014). In addition to this neurogenic activity, a profound angiogenic process takes place in the hypoxic CB (Wang and Bisgard, 2002; Chen et al., 2007a). Whether neural-crest-derived adult CB stem cells (CBSCs) are able to differentiate into vascular cells, contributing to angiogenesis in vivo, in addition to neurogenesis, is largely unknown. We have recently described the presence of mesectoderm-restricted progenitors within CB parenchyma and have shown that these cells are able to convert into endothelial cells in vitro (Navarro-Guerrero et al., 2016). Therefore, the CB constitutes an ideal model where to study the potential plasticity of an adult population of NCSCs.

Utilizing both in vitro assays and in vivo cell-fate mapping experiments, we show that adult CBSCs do indeed retain multipotent differentiation capacity, being able to convert into endothelial cells (ECs) contributing to hypoxia-induced angiogenesis during acclimatization of the organ. Moreover, we provide mechanistic insight into this process by showing that CBSCs differentiate into ECs via a hypoxia inducible factor (HIF)-dependent mechanism and in response to hypoxia-released molecules such as erythropoietin. Thus, CBSCs use plasticity to facilitate physiological adaptation of the CB, and hence the organism, to hypoxia.

RESULTS

CBSCs Differentiate Into Vascular Cell Types under Hypoxic Conditions

In order to test the ability of CBSCs to contribute to vascular cell types, we decided to perform in vivo cell-fate mapping using *GFAP-cre/floxed LacZ* or *YFP* transgenic mice. These animals express the β-galactosidase enzyme (β-gal), or the yellow fluorescent protein (YFP), in GFAP$^+$ CBSCs and their derivatives (Pardal et al., 2007). However, the human GFAP promoter in this type of construct is not expressed in all GFAP$^+$ mouse cells, as previously revealed in brain astrocytes (Malatesta et al., 2003). In the case of CB, a first exposure to hypoxia (7 days; Figure S1) needs to be performed in order to activate the construct (Pardal et al., 2007), and only around 50% of GFAP$^+$ CBSCs get labeled (Figure S1F). After this first exposure to hypoxia, only GFAP$^+$ CB stem cells and their derivatives in resting conditions, i.e., some nestin$^+$ progenitor cells, appear labeled (Figures S1G and S1H), confirming the specificity of the construct. After construct activation, we exposed *GFAP-cre/floxed LacZ* mice to hypoxia for 7 days (for hypoxic stimulus confirmation, see Figures 4K and S5C) and interrogated vascular cells for the expression of *LacZ*. By using an antibody against β-gal, and GSA I, an endothelium-specific lectin, we found that 16.3% ± 2.7% of ECs were positive for β-gal (39 out of 229 GSA I$^+$ cells analyzed; Figures 1A and S1J). No single β-gal$^+$ GSA I$^+$ cell was found in the

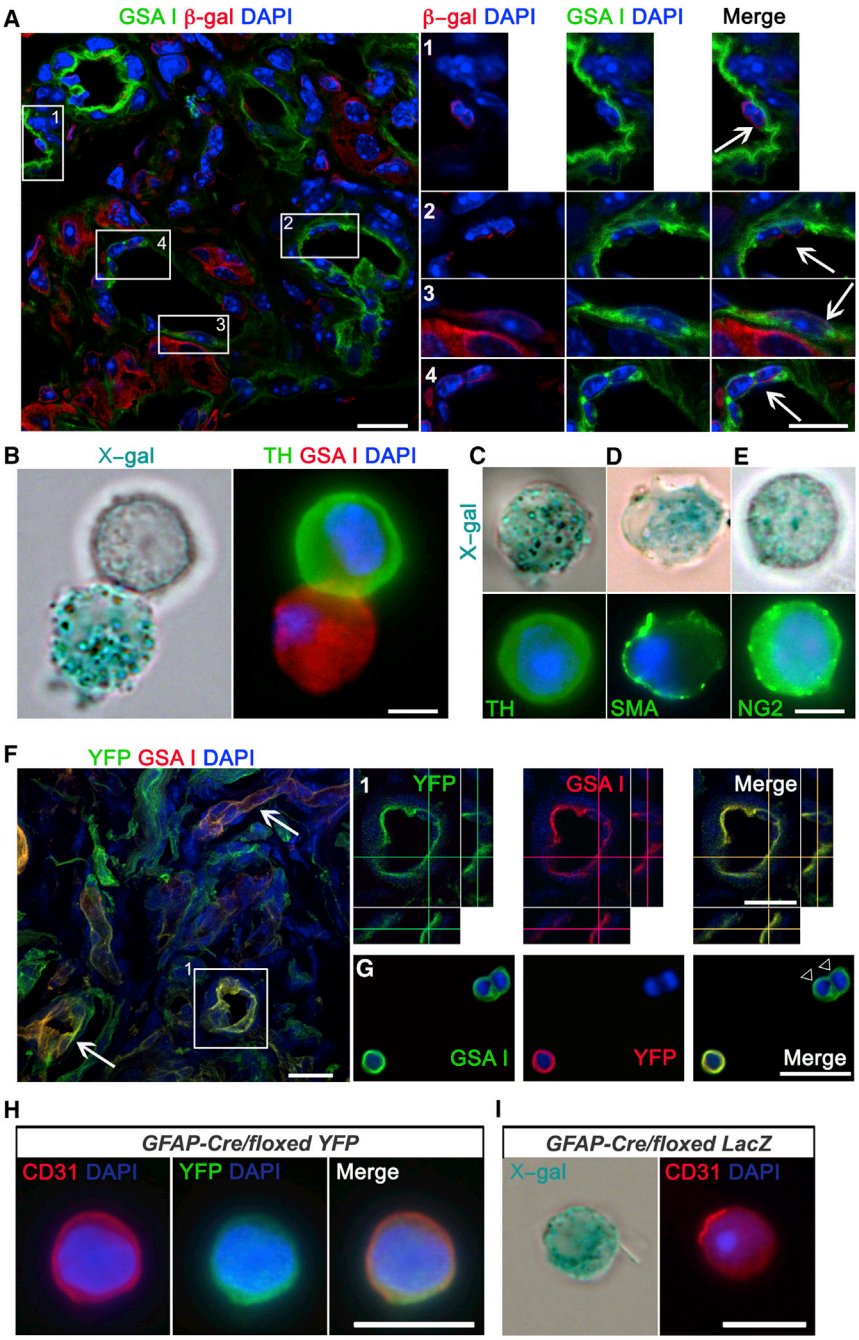

Figure 1. CB Stem Cells Contribute to Angiogenesis in Addition to Neurogenesis under Hypoxia

(A) Z stack projection picture obtained by confocal microscopy from a CB section of a hypoxic *GFAP-cre/floxed LacZ* mouse, immunostained with an antibody against β-galactosidase (red) and stained with the endothelial marker GSA I (green). ECs derived from GFAP$^+$ type II cells are shown in the enlargements of the boxed areas (arrows). Scale bars, 10 μm. Confocal pictures were taken in sections from two animals per group.

(B–E) Examples of X-gal$^+$ cells dispersed from the CB of hypoxic *GFAP-cre/floxed LacZ* mice. The pictures illustrate the appearance of X-gal$^+$ ECs (GSA I$^+$, B), glomus cells (TH$^+$, C), smooth muscle cells (SMA$^+$, D), and pericytes (NG2$^+$, E). Scale bars, 5 μm. n = 3 independent experiments.

(F) Fluorescence confocal microscopy pictures of CB sections from hypoxic *GFAP-cre/floxed YFP* mouse stained with anti-YFP antibody (green) and rodhamine-conjugated GSA I lectin. Arrows point to double-positive vessels. A higher magnification of the boxed region depicted in (F), showing z axis projection views, is shown in (1). Scale bars, 25 μm. n = 3 animals per experimental group.

(G) Picture of ex vivo hypoxic CB preparation stained with GSA I (green) and immunolabeled with an antibody against YFP reporter protein (red). Note the presence of GSA I positive ECs, negative for the reporter protein (white arrowheads). Scale bar, 25 μm.

(H and I) Examples of GFAP$^+$ cell-derived CD31$^+$ ECs, found in CB cell dispersions from both *GFAP-cre/floxed YFP* (H) and *GFAP-cre/floxed LacZ* (I) mice. Scale bars, 20 μm.

See also Figures S1 and S2.

CBs of normoxic *GFAP-cre/floxed LacZ* littermate mice (99 GSA I$^+$ cells analyzed), a result that was confirmed with YFP transgenic mice (Figure S1D). Differentiation of GFAP$^+$ CBSCs into ECs was confirmed in CB dispersed cells from hypoxic *GFAP-cre/floxed LacZ* mice, by using classical X-gal staining to reveal the activity of β-gal, and fluorescent cytochemistry to detect GSA I (Figure 1B), or the endothelial markers CD31 (Figure 1I), or von Willebrand factor (vWF; Figures S1K and S1L). Moreover, by using this CB ex vivo preparation, we confirmed neuronal differentiation capacity of GFAP$^+$ CBSCs in the same mice (Figure 1C). Interestingly, by using a smooth muscle cell marker (SMA; Figure 1D) and a pericyte marker (NG2; Figure 1E), we also uncovered the ability of CB neural progenitors to convert into other mesenchymal cell types forming the vascular compartment, suggesting that CB progenitors can give rise to complete blood vessels. The use of a second type of reporter mouse strain (*GFAP-cre/floxed YFP* mice) corroborated the cell-fate mapping results, both at the immunochemical (Figures 1F–1H) and flow cytometry (fluorescence-activated cell sorting [FACS]; Figure S1I) levels. The percentage of YFP$^+$ GSA I$^+$ cells, obtained from *GFAP-cre/floxed YFP* mouse CBs, was smaller (9.31% ± 0.59%) than from the *LacZ* mouse model, probably due to differences in Cre-mediated excision efficiencies between the two reporter genes used. The use of a different EC marker, such as CD31, for cell-fate mapping (Figures 1H, 1I, and S1I) yielded qualitatively very similar results. No single EC, labeled with the reporter gene, was found when analyzing the CB of *TH-Cre/floxed LacZ* mice (Figure S1M), ruling out an unspecific

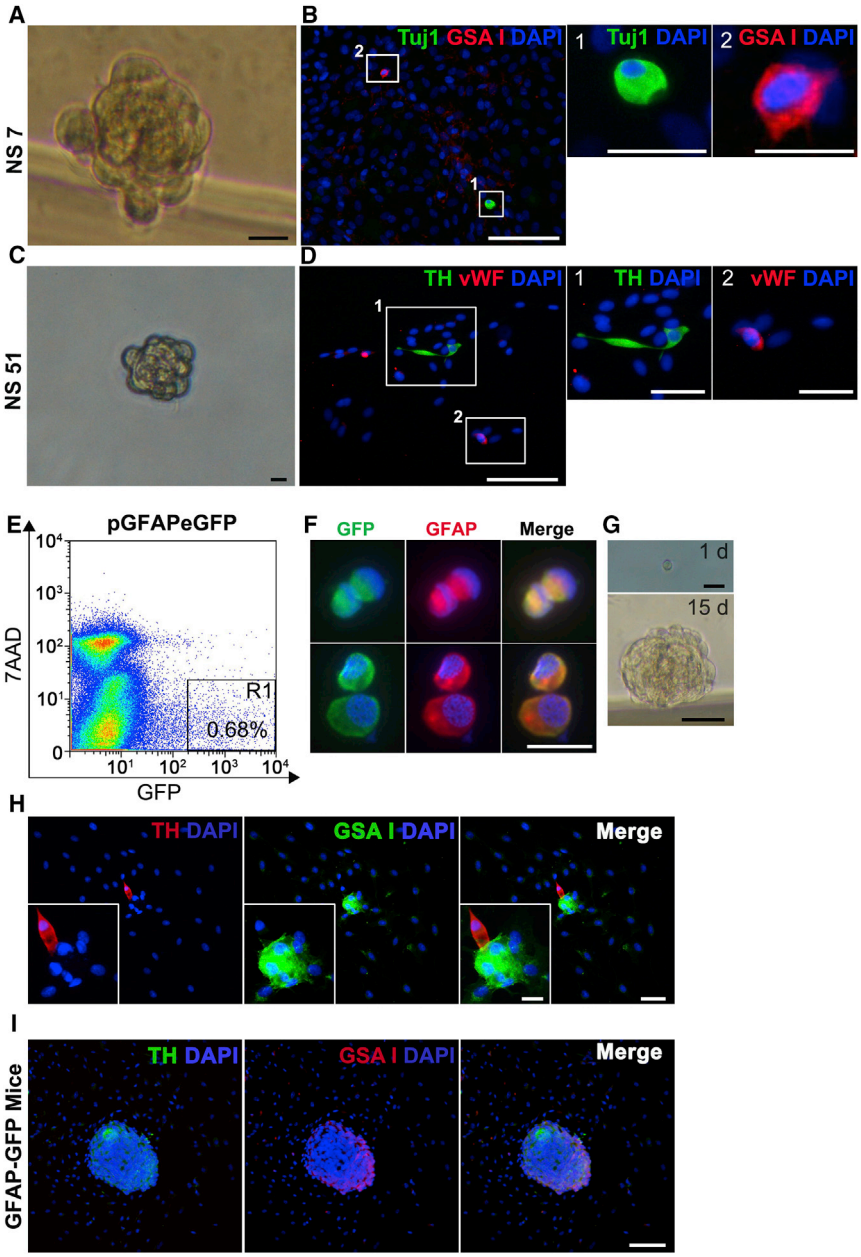

Figure 2. Single Progenitor Cells Display Multipotency In Vitro

(A and C) Bright-field photographs of secondary NS formed from single progenitors derived from enzymatic dispersion of primary NS. Scale bars, 5 μm.

(B and D) Immunofluorescence pictures of adherent secondary NS obtained from a single NS-derived progenitor cell (NSPC). Combinations of different cellular markers were tested inside the same colony (Tuj1 [green] and GSA I [red] in B, and TH [green] and vWF [red] in D). Scale bars, 100 μm. B1 and B2 and D1 and D2 show high-magnification images of the areas boxed in (B) and (D). Scale bars, 10 μm, in B1 and B2, and 30 μm, in D1 and D2. n = 4 primary NS cultures.

(E) Flow cytometry plot of dispersed rat CB cells transfected with *pGFAP-eGFP* plasmid.

(F) Image representing GFAP$^+$ cell enrichment in GFP$^+$ cell population sorted out by flow cytometry. Scale bar, 10 μm.

(G) Bright-field pictures showing the ability of single-cell plated GFP$^+$ cells (1 d) to form NS after 15 days (15 d) in culture. Scale bars, upper panel 10 μm and bottom panel 50 μm.

(H) Example of a single-cell-derived NS, containing cells of both neuronal (TH, red) and endothelial (GSA I, green) lineages. Scale bars, 10 μm, in (H), and 5 μm, in inset.

(I) Single-cell plating experiment performed using dispersed CB cells from *hGFAP-GFP* mice. Picture shows an example NS, double positive for neuronal (TH, green) and endothelial (GSA I, red) markers. Scale bar, 50 μm.

See also Figure S3.

expression of Cre recombinase by ECs, and confirming the differentiation of GFAP$^+$ CBSCs into vascular cells.

We corroborated the multipotent differentiation capacity of CBSCs in vivo, by performing bluo-gal staining and electron microscopy (EM) on the CB of hypoxic *GFAP-cre/floxed LacZ* mice (see Figure S2 and its legend). Altogether, in vivo cell-fate mapping experiments identify CBSCs as multipotent neural-crest-derived adult stem cells contributing to both neurogenesis and angiogenesis during hypoxic acclimatization of the organ.

Single CBSCs Display Multipotentiality In Vitro

To directly prove the multipotential capacity of CBSCs to differentiate into both neuronal and vascular cell types, we performed single-cell deposition experiments in vitro (Figure 2). Out of 1,536 dispersed primary neurosphere (NS) cells plated, 200 of them gave rise to secondary NS. Upon plating onto adherent conditions, 15 of those NS (7.5%) contained both neuronal and mesectodermal cells within the colony (Figures 2A–2D and S3A–S3F), confirming differentiation into both cell lineages from a single progenitor cell. The percentage of multipotent progenitor cells is likely being underestimated due to the lack of appropriate neuronal differentiation conditions in the single-cell plating assay. In addition to Tuj1 and GSA I markers (Figure 2B), we have corroborated the presence of neuronal and mesectodermal cells with different widely used markers: tyrosine hydroxylase (TH) for dopaminergic neuronal cells and vWF, NG2, and CD34 for vascular cells (Figures 2D and S3). We also performed single-cell plating analysis with FACS-sorted rat CB cells previously transfected with a *pGFAP-eGFP* construct, where 100% of GFP$^+$-sorted cells were GFAP$^+$ CBSCs (Figures 2E and 2F). Although the frequencies of NS formation and neuronal differentiation were quite low, likely due to transfection- and FACS-induced damage, and lack of optimal neuronal differentiation conditions, we were able to find some examples of

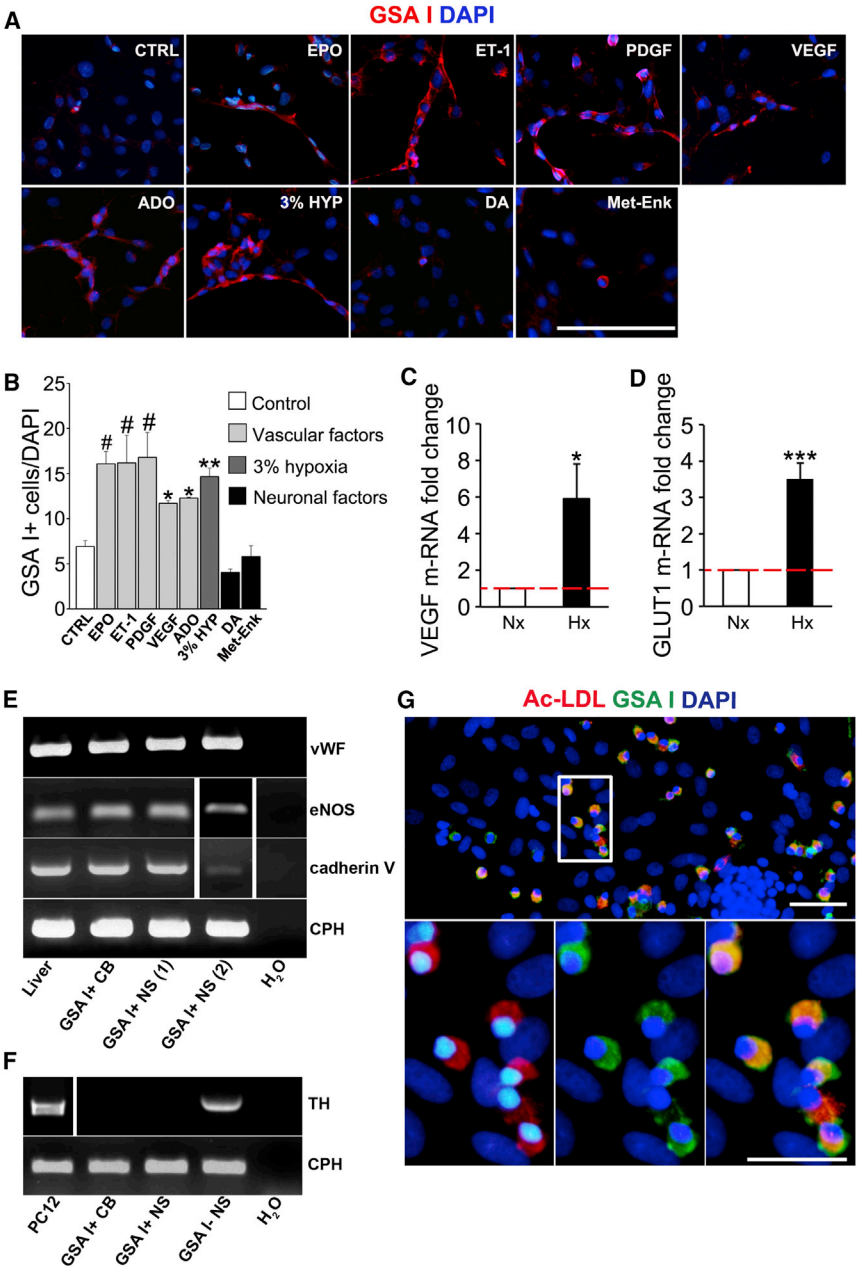

Figure 3. Vascular Factors Increase CBSC Endothelial Differentiation In Vitro

(A) Epifluorescent detection of GSA I (ECs; red) in adherent NS cultured on fibronectin in standard neural crest culture medium without mitogens (CTRL) and supplemented with vascular or neuronal factors. Scale bar, 200 μm.

(B) Quantification graph indicating the mean percentage of GSA I$^+$ cells among total cells in different culture conditions. Data are represented as the mean ± SEM.; *p ≤ 0.05, **p ≤ 0.01; # p ≤ 0.001, one-way ANOVA Newman-Keuls post hoc test compared to CTRL measurement. n = from three to nine independent NS cultures.

(C and D) Graphs representing a significant increase in mRNA expression of two classical hypoxia-inducible genes, VEGF (C) and GLUT1 (D). n = 4 independent NS cultures. In vitro hypoxia experiments were performed at 3% O_2. Data are represented as mean ± SEM.

(E) RT-PCRs revealing expression of mature endothelial markers in rat liver and in GSA I$^+$ cells isolated from CB or adherent NS by flow cytometry.

(F) Agarose gel showing TH mRNA amplified by RT-PCR in GSA - cell fraction isolated from adherent NS. Three independent RNA extractions were tested for each gene expression analysis.

(G) Binding of FITC-GSA I and uptake of Dil-acetylated LDL (Ac-LDL) in ECs in vitro, visualized by fluorescence microscopy. Nuclei are counterstained with DAPI (blue). Scale bars, 50 μm (top) and 25 μm (bottom). n = 3 NS cultures.

See also Figures S3, S4, and S6.

multipotent differentiation from single CBSCs (Figures 2G and 2H). Consistently, we also found multipotent differentiation when plating single GFP$^+$ cells from CBs of *GFAP-eGFP* transgenic mice (Figure 2I). Altogether, our single-cell plating data confirm multipotent differentiation capacity in CBSCs.

CBSCs Are Sensitive to Vascular Factors and Differentiate into Functional ECs

We next decided to explore the mechanisms by which CBSCs differentiate into ECs by using in vitro assays and rat CB cells, since the organ in rats is more manageable than in mice and the cells grow better in culture. Rat CBSC-derived NS can be plated onto adherent conditions where, upon mitogen withdrawal, cells are induced to differentiate. Using this assay, we found that CB progenitors differentiate into ECs (GSA I$^+$) when exposed to adherent substrate (control in Figures 3A and 3B). However, this differentiation was dramatically enhanced when the cells were exposed to hypoxia (see Figures 3C and 3D for hypoxia confirmation in vitro) or vascular factors (Figures 3A and 3B), such as erythropoietin (EPO), endothelin-1 (ET-1), platelet-derived growth factor (PDGF), vascular endothelial growth factor (VEGF), or adenosine (ADO). This differentiation effect appeared to be specific for vascular factors since the addition of typical CB neuronal factors, such as dopamine (DA) or methionine-enkephalin (Met-Enk) (González-Guerrero et al., 1993; Gauda and Gerfen, 1996), did not increase endothelial differentiation (Figures 3A and 3B). Interestingly, most vascular factors studied are consistently expressed in CB ECs, as assessed by RT-PCR on FACS-sorted CB cells (Figure S3H).

We next evaluated the expression of mature EC markers in GSA I$^+$ NS cells, using GSA I$^+$ CB dispersed cells and liver cells as positive controls (Figure 3E). We confirmed the expression of vWF, endothelial NO synthase (eNOS), and cadherin V, all of

them specific for mature endothelium. We also confirmed the expression of the receptors for the different vascular factors that activate endothelial differentiation in CBSCs (Figure S3I). Both CB- and NS-derived GSA I^+ cells lack expression of the receptor for DA (DRD2; Figure S3J), a neurotransmitter that did not increase endothelial differentiation (Figures 3A and 3B). As a control, we tested the expression of a CB neuronal marker (TH; Figure 3F), corroborating the lack of neuronal cell contamination in GSA I^+ populations. Moreover, we studied the functionality of CBSC-derived ECs obtained in vitro, by performing a low-density lipoprotein (LDL) uptake assay (Voyta et al., 1984). Out of 216 GSA I^+ cells analyzed from three independent cultures, 95% ± 1.5% of them were also positive for DiI-conjugated Ac-LDL (Figure 3G), confirming the uptake and intracellular storage of lipoproteins, and hence the functionality of ECs differentiated from CBSCs in vitro. Finally, we decided to confirm the vasculogenic capacity of CB progenitor cells by using Matrigel and a subcutaneous vasculogenesis assay (see Figure S4). Taken together, in vitro and in vivo functional assays and endothelial marker expression analysis indicate that neural-crest-derived CBSCs are able to differentiate into mature and functional ECs, supporting their capacity to participate in CB angiogenesis.

Endothelial Differentiation from CBSCs Is HIF Dependent and Sensitive to EPO

Interestingly, in vitro differentiation assays indicate that CBSC conversion into ECs is directly favored by low oxygen (see Figure 3A). Therefore, we decided to check whether CBSCs were intrinsically sensitive to hypoxia, and whether prolyl hydroxylase (PHD)/HIF pathway had a role in the vascular differentiation process. Our data (see Figure S5) clearly establish an important, although partial, role for HIF2α in the endothelial differentiation process. In addition, we decided to further study the role of a relevant hypoxia-induced vascular cytokine, EPO. EPO is a hematopoietic factor, finely regulated by oxygen tension (Franke et al., 2013), that has been described to participate in angiogenesis (Heeschen et al., 2003). In vitro results described above show that EPO increases the number of ECs obtained from CBSCs (see Figures 3A and 3B), and this is achieved without affecting neuronal differentiation (Figures 4A and 4B). Moreover, EPO receptor (EPOR) is expressed by both NS- and CB-derived nestin$^+$-activated progenitors (Figure 4C), suggesting a direct role of this cytokine on CBSC fate determination. Therefore, we decided to further examine the role of EPO on CB angiogenesis both in vitro and in vivo. The addition to adherent NS cultures of an antibody against EPO, that sequesters the hematopoietic cytokine, completely abrogated the increase in endothelial differentiation (Figures 4D and 4E). AG490 is an inhibitor of EPOR-associated Janus kinase (Jak) 2 that has been described to block EPO intracellular signaling (Lester et al., 2005). Addition of AG490 to EPO-treated adherent NS provoked a significant decrease in the number of ECs obtained (Figures 4D and 4E). Thus, our results suggest a specific role for EPO in the induction of endothelial differentiation from CBSCs in vitro.

We then decided to corroborate that EPO was being endogenously produced in the CB (Lam et al., 2009). As assessed by RT-PCR, CB cells produce EPO especially in hypoxic conditions (Figure 4F). In order to test whether cell-released EPO was able to direct vascular differentiation from CB progenitors, we performed hypoxic co-cultures of NS progenitor cells and ECs (Figure 4G). For these co-culture experiments, we used a well-characterized human EC line (HUVEC), which produces EPO (Figure 4H). The presence of HUVECs in the surrounding wells increased the amount of functional ECs in CB NS, an effect that was abrogated after the addition of a blocking antibody against EPO (Figures 4I and 4J), further corroborating the role of EPO on CB progenitor endothelial differentiation in vitro.

Finally, we wanted to test whether EPO was having a relevant role in hypoxia-induced CB angiogenesis in vivo. To this end, we used *GFAP-cre/floxed LacZ* transgenic mice exposed to hypoxia. Systemic injection of EPO signaling blocker AG490 in these mice significantly attenuated the typical hypoxia-induced EPO-mediated hematocrit increase (Figure 4K), corroborating the systemic action of the inhibitor. CBSC-derived newly formed ECs are labeled by β-galactosidase expression and hence appear with blue precipitate after X-gal staining (Figure 4L). Quantification of X-gal$^+$ cells in dispersed CB of these AG490-treated hypoxic mice revealed a decrease in the number of GSA I^+ ECs derived from CBSCs (Figure 4M), confirming the importance of EPO release and EPO signaling in CBSC-dependent angiogenesis.

DISCUSSION

In the present study, we show that adult CBSCs display multipotent differentiation capacity, giving rise to both neural and non-neural derivatives during physiological acclimatization of CB to hypoxia. Our results show that around 10%–15% of total ECs, after a single exposure of the organ to chronic hypoxia, are derived from CBSCs, and this value is likely being underestimated due to inefficient expression of transgenic constructs (Figure S1). Considering that ECs are described to double their number in the organ in response to hypoxia (Chen et al., 2007a), we therefore estimate that around one every three or four newly formed ECs is CBSC derived.

The ability of NSCs to differentiate into ECs has been previously described only in some in vitro studies (Wurmser et al., 2004; Ii et al., 2009) or in the context of nervous system oncological disease (Ricci-Vitiani et al., 2010; Wang et al., 2010; Pezzolo et al., 2011; Cheng et al., 2013). However, to the best of our knowledge, no other example has been reported about adult neural progenitors participating in a physiological process of angiogenesis in vivo.

In addition to the direct effect of hypoxia (see the role of HIF2α in the Supplemental Information), conversion of CBSCs into ECs is also clearly enhanced by the exposition of cells to vascular factors, which are particularly released during hypoxia (Fandrey, 1995). Among these factors, EPO has been described to regulate CNS progenitor behavior (Shingo et al., 2001; Chen et al., 2007b) and has a clear role enhancing vasculogenesis (Bahlmann et al., 2004; Wang et al., 2004). Our results show that CB cells produce this vascular factor mainly during hypoxia, indicating that locally produced EPO might play a role in angiogenesis in the CB. This result is consistent with the described production of EPO by neuronal glomus cells in the organ (Lam et al., 2009). Moreover, we have recently described a role for CB neuronal cells on the

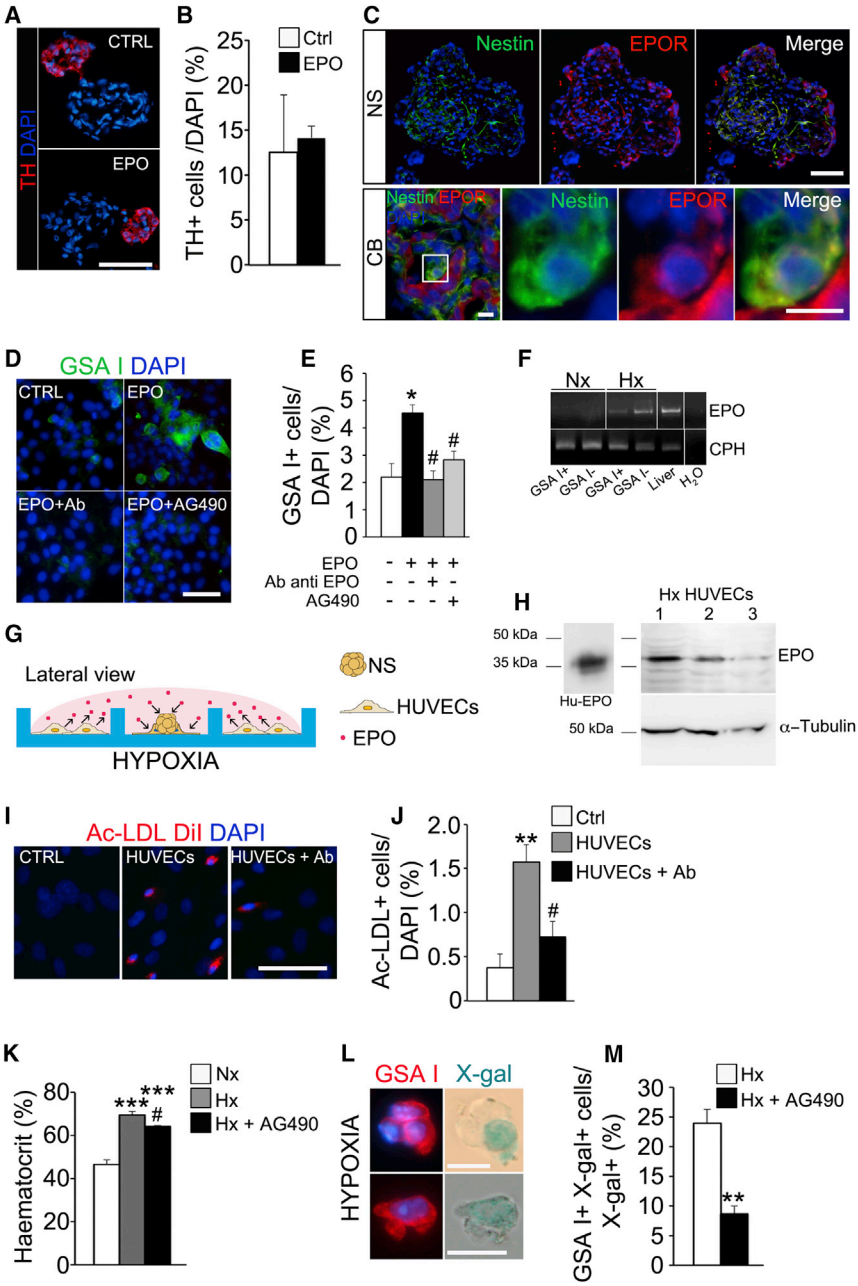

Figure 4. EPO Promotes the Endothelial Differentiation Capacity of CBSCs

(A) Immunohistochemistry pictures illustrating the size of TH$^+$ neuronal blebs in control and EPO-exposed NS. Scale bar, 50 μm.

(B) Quantification of the percentage of TH$^+$ cells versus total cells in NS sections, comparing control and EPO-treated NS. Data are represented as the mean ± SEM. No statistical differences were detected by Student's t test.

(C) Immunofluorescence pictures showing presence of EPO receptor (EPOR) on the surface of nestin$^+$ progenitors in both NS (upper panels) and CB (lower panels) tissues. Scale bars, 50 μm, in upper panels, and 10 μm, in lower panels.

(D) Images displaying EC differentiation within adherent cultures of primary NS in presence of EPO, EPO combined with EPO neutralizing antibody, or EPOR inhibitor (AG490). Scale bar, 50 μm.

(E) Quantification graph indicating the mean percentage of GSA I$^+$ cells in different culture conditions. Data are represented as the mean ± SEM; *p ≤ 0.05, one-way ANOVA Newman-Keuls post hoc test compared to control measurement (white bar), and #p ≤ 0.05, one-way ANOVA Newman-Keuls post hoc test compared to EPO treated measurement (black bar) (n = 3 cultures).

(F) Agarose gel showing the presence of EPO mRNA in hypoxic CB samples. n = 3.

(G) Schematic diagram describing the co-culture experiment.

(H) Representative western blot detecting EPO in three different hypoxic HUVEC protein extracts. The antibody recognizes in the cell extracts a band of about 38 kDa in concordance with human recombinant EPO (Hu-EPO).

(I) Pictures showing EC differentiation, detected by intracellular DiI-Ac-LDL uptake, occurring in NSPCs in different co-culture conditions. Parallel NS cultures without HUVECs served as control (CTRL). Scale bar, 25 μm.

(J) Quantification graph showing the percentage of DiI-Ac-LDL$^+$ cells detected in different co-culture conditions. Data are represented as the mean ± SEM.; **p ≤ 0.01, one-way ANOVA Newman-Keuls post hoc test compared to Ctrl measurement; #p ≤ 0.05, one-way ANOVA Newman-Keuls post hoc test compared to HUVEC co-culture measurement (n = 4 cultures).

(K) Histogram representing the significant increase of hematocrit, a typical hypoxia-sensitive EPO-mediated physiological variable, in experimental hypoxic animals (gray bar, n = 5) versus normoxic animals (white bar, n = 4). Consistently, treatment of hypoxic animals with EPOR inhibitor AG490 produced a significant decrease of hematocrit levels (black bar) when compared to hypoxia. In vivo experiments were carried out at 10% O_2. Data are represented as mean ± SEM.

(L) Representative microphotographs of X-gal$^+$ GSA I$^+$ cells observed in dispersed CB from *GFAP Cre/floxed LacZ* mice exposed to hypoxia for 7 days. Scale bars, 10 μm.

(M) Quantification of the percentage of X-gal$^+$ GSA I$^+$ cells versus total X-gal$^+$ cells found in dissociated CBs from *GFAP Cre/floxed LacZ* mice injected with vehicle (n = 3) or AG490 (n = 3), after 7 days of hypoxic treatment. **p ≤ 0.01, Student's t test compared to vehicle-treated hypoxic animals. Data are represented as mean ± SEM.

See also Figures S5 and S6.

proliferative activation of CBSCs through a different cytokine, ET-1 (Platero-Luengo et al., 2014). The additional release of EPO by CB glomus cells might represent another example of neuronal activity-dependent regulation of stem cell behavior, in this case promoting progenitors to participate in angiogenesis. Nevertheless, we cannot formally discard an additional role for circulating EPO in CB angiogenesis. Altogether, our results suggest that CBSCs retain mesectodermal differentiation potential,

resembling neural progenitors in the peripheral nervous system during development (Le Douarin et al., 2008). This ability allows them to participate in physiological angiogenesis, in addition to neurogenesis, during adaptation of the organ to hypoxia. This finding might be relevant to understand the pathophysiology of this chemoreceptor organ and to improve the therapeutic use of these stem cells.

EXPERIMENTAL PROCEDURES

Animals

Male and female transgenic mice (4–6 weeks old or 8–9 months old for dimethyloxalylglycine [DMOG] in vivo experiments) and Wistar rats (6 weeks old) were housed and treated according to the animal care guidelines of the European Community Council (86/609/EEC). All experimental procedures were approved by the Committee on Animal Research at the University of Seville. Details about the hypoxic treatment and drug administration are given in the Supplemental Information.

Dissociation of CB Cells and NS Cultures

Rat and transgenic mouse CBs were dissociated by enzymatic treatment and cultured to form NS, following protocols previously described (Pardal et al., 2007). Specific details are given in the Supplemental Information.

Immunocytochemistry and Immunohistochemistry

Immunostainings were performed following standard procedures described elsewhere (Pardal et al., 2007). Antibodies used are listed in Table S1. Specific details about the immunostaining protocols are given in the Supplemental Information.

X-Gal Staining

Dispersed CB cells from *GFAP-cre/floxed LacZ* and *TH-cre/floxed LacZ* mice were plated in ultralow binding Petri dishes and allowed to recover superficial epitopes, lost upon enzymatic dispersion, in an incubator overnight. After that, standard protocols for X-gal staining were applied, as previously described (Pardal et al., 2007). Once X-gal staining was performed, we processed the cells for antibody staining as indicated previously.

EM

Carotid bifurcations were embedded in gelatin (80–100 bloom; Panreac) supplemented with 2% glutaraldehyde (Electron Microscopy Sciences), and 50-μm-thick slices were cut on a vibratome (VT1000S; Leica Microsystems). CB vibratome sections were processed for bluo-gal staining. Specific details about this staining are given in the Supplemental Information.

In Vitro Multipotency Assay

Primary NS were collected in 15-mL conical tubes and centrifuged at 100 × *g* for 1 min. Following aspiration of supernatant, NS were dispersed by Accutase (Sigma), gently pipetting up and down during 10 min. After enzymatic treatment, 4 mL of medium was added to quench enzymes. Dissociated NS cells were centrifuged for 5 min at 300 × *g* at 4°C. Afterward, cells were resuspended and cultured at clonal density on an ultralow binding 96-well plate. Secondary NS were re-plated onto adherent conditions using fibronectin pre-treated plates, as described before. After 3 days in culture, adherent NS colonies were fixed in 4% paraformaldehyde (PFA) and processed for immunolabeling and GSA I staining (see above).

Endothelial Differentiation Assay

NS obtained from dispersed rat CBs were re-plated onto adherent conditions using 5 μg/mL fibronectin (Biomedical Technologies) pre-treated 24-well plates, at a density of 4 or 5 NS/well. Drug treatments are described in the Supplemental Information. After growing for 3 days in adherent conditions, flat NS colonies were fixed and stained with rodhamine or fluorescein-conjugated GSA I (see Immunocytochemistry section). ImageJ software (National Institute of Health) was used for cell number quantifications.

RT-PCR and Real-Time qPCR

Total RNA was extracted from GSA I positive and negative cell fractions from dispersed adherent NS or dispersed rat CBs, using a commercial kit (RNeasy MICRO kit; QIAGEN), following manufacturer's instructions. For retrotranscription, cDNA was synthesized with QuantiTec Reverse transcription kit (QIAGEN), as indicated by manufacturer's instructions. Primer sequences are reported in Table S2. Original gels for all PCRs are shown in Figure S6.

Flow Cytometry

All sorts and analysis were performed in a MoFlo three-laser flow cytometer (DAKO Cytomation) and a LSR Fortessa (BD Biosciences), respectively. Specific details about flow cytometry protocols are given in the Supplemental Experimental Procedures.

Western Blot

Whole-cell protein extracts were obtained from HUVEC cell line, cultured during 3 days in hypoxic conditions (3% O_2) in EC basal medium-2 (EBM-2, Lonza) for EPO protein detection. Specific details about the western blot protocol are given in the Supplemental Experimental Procedures.

Statistics

Analyses of significant differences between means were carried out using the unpaired or paired two-tailed Student's t test. Newman-Keuls post hoc or Tukey's multiple comparison tests were used whenever a significant difference between three or more sample means was revealed by a one-way ANOVA. Tukey or Newman-Keuls test was used depending upon whether or not additional power is required to detect significant differences between means. p values ≤ 0.05 were considered significant. More details about the statistical analysis are given in the Supplemental Information.

SUPPLEMENTAL INFORMATION

Supplemental Information includes Supplemental Experimental Procedures, six figures, and two tables and can be found with this article online at http://dx.doi.org/10.1016/j.celrep.2017.03.065.

AUTHOR CONTRIBUTIONS

R.P. and V.A. designed the experiments. V.A. conducted most of the experiments. E.N.-G. and I.R.-P. assisted V.A. with some of the experiments. R.P. and V.A. wrote the paper.

ACKNOWLEDGMENTS

We thank CITIUS and María José Castro for technical assistance. We thank Ángela Molina for help with PCRs, Professor Andreas Brech for his scientific advice, Juan Francisco Martín Rodríguez for help with Statistics, and José I. Piruat, José López Barneo, and David Cano for their valuable comments on the manuscript. This research was supported by European grants (ERC Starting Grant: CBSCs) and by Spanish Ministry of Economy and Competitiveness grant (SAF2013-48535-P and SAF2016-80412-P). V.A. was supported by a Juan de la Cierva fellowship from the Spanish Ministry of Economy and Competitiveness.

Received: September 30, 2016
Revised: February 21, 2017
Accepted: March 27, 2017
Published: April 18, 2017

REFERENCES

Arias-Stella, J., and Valcarcel, J. (1976). Chief cell hyperplasia in the human carotid body at high altitudes; physiologic and pathologic significance. Hum. Pathol. *7*, 361–373.

Bahlmann, F.H., De Groot, K., Spandau, J.M., Landry, A.L., Hertel, B., Duckert, T., Boehm, S.M., Menne, J., Haller, H., and Fliser, D. (2004). Erythropoietin regulates endothelial progenitor cells. Blood *103*, 921–926.

Chen, J., He, L., Liu, X., Dinger, B., Stensaas, L., and Fidone, S. (2007a). Effect of the endothelin receptor antagonist bosentan on chronic hypoxia-induced morphological and physiological changes in rat carotid body. Am. J. Physiol. Lung Cell. Mol. Physiol. *292*, L1257–L1262.

Chen, Z.Y., Asavaritikrai, P., Prchal, J.T., and Noguchi, C.T. (2007b). Endogenous erythropoietin signaling is required for normal neural progenitor cell proliferation. J. Biol. Chem. *282*, 25875–25883.

Cheng, L., Huang, Z., Zhou, W., Wu, Q., Donnola, S., Liu, J.K., Fang, X., Sloan, A.E., Mao, Y., Lathia, J.D., et al. (2013). Glioblastoma stem cells generate vascular pericytes to support vessel function and tumor growth. Cell *153*, 139–152.

Edwards, C., Heath, D., and Harris, P. (1971). The carotid body in emphysema and left ventricular hypertrophy. J. Pathol. *104*, 1–13.

Fandrey, J. (1995). Hypoxia-inducible gene expression. Respir. Physiol. *101*, 1–10.

Franke, K., Gassmann, M., and Wielockx, B. (2013). Erythrocytosis: The HIF pathway in control. Blood *122*, 1122–1128.

Gauda, E.B., and Gerfen, C.R. (1996). Expression and localization of enkephalin, substance P, and substance P receptor genes in the rat carotid body. Adv. Exp. Med. Biol. *410*, 313–318.

González-Guerrero, P.R., Rigual, R., and González, C. (1993). Opioid peptides in the rabbit carotid body: Identification and evidence for co-utilization and interactions with dopamine. J. Neurochem. *60*, 1762–1768.

Heath, D., Smith, P., and Jago, R. (1982). Hyperplasia of the carotid body. J. Pathol. *138*, 115–127.

Heeschen, C., Aicher, A., Lehmann, R., Fichtlscherer, S., Vasa, M., Urbich, C., Mildner-Rihm, C., Martin, H., Zeiher, A.M., and Dimmeler, S. (2003). Erythropoietin is a potent physiologic stimulus for endothelial progenitor cell mobilization. Blood *102*, 1340–1346.

Ii, M., Nishimura, H., Sekiguchi, H., Kamei, N., Yokoyama, A., Horii, M., and Asahara, T. (2009). Concurrent vasculogenesis and neurogenesis from adult neural stem cells. Circ. Res. *105*, 860–868.

Lam, S.Y., Tipoe, G.L., and Fung, M.L. (2009). Upregulation of erythropoietin and its receptor expression in the rat carotid body during chronic and intermittent hypoxia. Adv. Exp. Med. Biol. *648*, 207–214.

Le Douarin, N.M., Calloni, G.W., and Dupin, E. (2008). The stem cells of the neural crest. Cell Cycle *7*, 1013–1019.

Lester, R.D., Jo, M., Campana, W.M., and Gonias, S.L. (2005). Erythropoietin promotes MCF-7 breast cancer cell migration by an ERK/mitogen-activated protein kinase-dependent pathway and is primarily responsible for the increase in migration observed in hypoxia. J. Biol. Chem. *280*, 39273–39277.

López-Barneo, J., Pardal, R., and Ortega-Sáenz, P. (2001). Cellular mechanism of oxygen sensing. Annu. Rev. Physiol. *63*, 259–287.

Malatesta, P., Hack, M.A., Hartfuss, E., Kettenmann, H., Klinkert, W., Kirchhoff, F., and Götz, M. (2003). Neuronal or glial progeny: Regional differences in radial glia fate. Neuron *37*, 751–764.

Navarro-Guerrero, E., Platero-Luengo, A., Linares-Clemente, P., Cases, I., López-Barneo, J., and Pardal, R. (2016). Gene Expression Profiling Supports the Neural Crest Origin of Adult Rodent Carotid Body Stem Cells and Identifies CD10 as a Marker for Mesectoderm-Committed Progenitors. Stem Cells *34*, 1637–1650.

Pardal, R., Ortega-Sáenz, P., Durán, R., and López-Barneo, J. (2007). Glia-like stem cells sustain physiologic neurogenesis in the adult mammalian carotid body. Cell *131*, 364–377.

Pezzolo, A., Parodi, F., Marimpietri, D., Raffaghello, L., Cocco, C., Pistorio, A., Mosconi, M., Gambini, C., Cilli, M., Deaglio, S., et al. (2011). Oct-4+/Tenascin C+ neuroblastoma cells serve as progenitors of tumor-derived endothelial cells. Cell Res. *21*, 1470–1486.

Platero-Luengo, A., González-Granero, S., Durán, R., Díaz-Castro, B., Piruat, J.I., García-Verdugo, J.M., Pardal, R., and López-Barneo, J. (2014). An O2-sensitive glomus cell-stem cell synapse induces carotid body growth in chronic hypoxia. Cell *156*, 291–303.

Ricci-Vitiani, L., Pallini, R., Biffoni, M., Todaro, M., Invernici, G., Cenci, T., Maira, G., Parati, E.A., Stassi, G., Larocca, L.M., and De Maria, R. (2010). Tumour vascularization via endothelial differentiation of glioblastoma stem-like cells. Nature *468*, 824–828.

Shingo, T., Sorokan, S.T., Shimazaki, T., and Weiss, S. (2001). Erythropoietin regulates the in vitro and in vivo production of neuronal progenitors by mammalian forebrain neural stem cells. J. Neurosci. *21*, 9733–9743.

Voyta, J.C., Via, D.P., Butterfield, C.E., and Zetter, B.R. (1984). Identification and isolation of endothelial cells based on their increased uptake of acetylated-low density lipoprotein. J. Cell Biol. *99*, 2034–2040.

Wang, Z.Y., and Bisgard, G.E. (2002). Chronic hypoxia-induced morphological and neurochemical changes in the carotid body. Microsc. Res. Tech. *59*, 168–177.

Wang, L., Zhang, Z., Wang, Y., Zhang, R., and Chopp, M. (2004). Treatment of stroke with erythropoietin enhances neurogenesis and angiogenesis and improves neurological function in rats. Stroke *35*, 1732–1737.

Wang, R., Chadalavada, K., Wilshire, J., Kowalik, U., Hovinga, K.E., Geber, A., Fligelman, B., Leversha, M., Brennan, C., and Tabar, V. (2010). Glioblastoma stem-like cells give rise to tumour endothelium. Nature *468*, 829–833.

Wurmser, A.E., Nakashima, K., Summers, R.G., Toni, N., D'Amour, K.A., Lie, D.C., and Gage, F.H. (2004). Cell fusion-independent differentiation of neural stem cells to the endothelial lineage. Nature *430*, 350–356.